Surface & Coatings Technology 404 (2020) 126643

Contents lists available at ScienceDirect

Surface & Coatings Technology

journal homepage: www.elsevier.com/locate/surfcoat

Cobalt thin films as water-recombination electrocatalysts

Clara Linder [a,b], Smita Gangaprasad Rao [c], Arnaud le Febvrier [c], Grzegorz Greczynski [c], Rune Sjövall [d], Sara Munktell [e], Per Eklund [c], Emma M. Björk [b,*]

[a] RISE, Corrosion, Vehicles and Surface Protection, 164 40 Kista, Sweden
[b] Nanostructured Materials, Department of Physics, Chemistry and Biology (IFM), Linköping University, 581 83 Linköping, Sweden
[c] Thin Film Physics Division, Department of Physics, Chemistry, and Biology (IFM), Linköping University, 581 83 Linköping, Sweden
[d] SAFT AB, 572 28 Oskarshamn, Sweden
[e] Swerim AB, Metallic Materials in Corrosive Environments, 164 40 Kista, Sweden

ARTICLE INFO

Keywords:
Cobalt thin film
Anodization
Cobalt oxide
Electrocatalyst
Oxygen reduction reaction
Water recombination

ABSTRACT

Catalysts and electrocatalysts are crucial for energy production and storage. To develop cost-efficient systems taking advantage of functionalized surfaces, the catalysts can be synthesized as nanomaterials or thin films. In this work, cobalt thin films were deposited on low-alloyed steel using magnetron sputtering. The films are uniform with a smooth surface and a thickness of ~400 nm. The films were electrochemically oxidized via anodization to a mix of cobalt oxides, one of them being Co_3O_4, at room temperature in an alkaline solution. The electrocatalytic performances of the anodized films were evaluated in 1 M KOH electrolyte saturated with oxygen. Cathodic currents in −0.5 mA/cm^2 range, corresponding to oxygen reduction reaction (ORR) activity, were measured with cyclic voltammetry. The catalytic activity of the films was evaluated as a function of time. The anodized Co coating exhibited three times higher activity than the steel substrate. The kinetics for the ORR were evaluated through Tafel plots and a slope of 226 mV/decade was found. Post-ORR characterization of the films revealed hexagonal plate-like oxide particles on the surface. After 50 cyclic voltammograms, the film was further oxidized, indicating that the ORR activity also affects the overall surface state of the film. This study demonstrates that thin films, after electrochemical modification, can be electrocatalysts for the oxygen reduction reaction and potentially used for applications in energy production and storage.

1. Introduction

To find alternatives to fossil fuels, technologies including water recombination have been developed. These technologies are found in devices such as proton exchange membrane (PEM) or solid oxide fuel cells but can also be a necessity for batteries with water-based electrolytes [1]. Water recombination involves exchange of electrons when hydrogen and oxygen sources are combined together to reform water. The recombination is divided into oxygen reduction reaction (ORR) and hydrogen oxidation reaction (HOR). For these reactions to occur there is a need for an electron transfer medium, typically a carbon electrode. However, due to the sluggish kinetics of ORR [2], these reactions have an extremely low reaction rate. Therefore, an electrocatalyst is required for devices driven by water recombination to function with high efficiency. In industrial devices, the catalytically active material must be present on large surfaces, e.g., bipolar plates or electrodes. Hence, coating the surfaces with a thin film is an appropriate approach [3].

For ORR and oxygen evolution reaction (OER), there is either a direct or indirect pathway. Four electrons are to be transferred in the direct pathway to reduce oxygen gas molecules to hydroxide ions. An indirect pathway involves a middle reaction usually with formation of peroxide ions HO_2^- with two electrons transferred twice with the same final product hydroxide ions OH^- [4].

Several materials have been used for these reactions. Noble metals such as Pt and Pd are excellent catalyst candidates with the highest activity for ORR [2,5], but due to their high cost and scarcity there is a need for replacing these precious metals. To reduce the amount of Pt it is possible to combine it with 3d transition metals [6], but for a larger scale production the required quantity of Pt is still too high. The utilization of 3d transition metals catalysts and their corresponding oxides without precious metals in ORR have therefore been extensively studied [2,7–9]. One of these 3d transition metals is cobalt, and cobalt oxides such as Co_3O_4 nanoparticles have presented good catalytic activity for ORR [10], in some cases even as high as noble metal-based catalysts [5].

* Corresponding author.
E-mail address: emma.bjork@liu.se (E.M. Björk).

https://doi.org/10.1016/j.surfcoat.2020.126643
Received 21 August 2020; Received in revised form 21 October 2020; Accepted 10 November 2020
Available online 17 November 2020

Co_3O_4 can have a spinel structure, meaning that Co^{2+} and Co^{3+} cations are placed in tetrahedral and octahedral interstitial sites of an FCC O^{2-} structure. Co cations in the spinel allow adsorption/desorption mechanisms and electron transfer suitable for ORR and OER [2,11]. Synthesis of Co_3O_4 can be carried out in various ways; from Co hydroxide precursors in solutions, by oxide formation through annealing at high temperature, or by electrochemical processes [12,13]. Tailoring the size of the spinel nano-particles leads to higher surface area and, thus, more active sites and higher catalytic activity [9]. Additionally, Co_3O_4 is stable at high pH and therefore applicable to alkaline processes, i.e. in alkaline batteries [14]. Liang et al. [13] synthesized Co_3O_4 nanoparticles on graphene sheets and found excellent ORR and OER activity in 0.1 M KOH. The hybrid nanoparticles had low overpotential and a high current density. Co_3O_4 has been further investigated for its ORR and OER properties. For example, Menezes et al. [5] produced Co_3O_4 nano-chains and compared ORR activities with other Co_3O_4 nanoparticles with different morphologies. The Co_3O_4 nano-chains showed good performances for both ORR and OER reactions. Xu et al. [4] studied carbon supported Co_3O_4 nano-rods and compared the performances with Pd for fuel cell applications. They demonstrated that the Co_3O_4 activity and electrochemical behaviour is similar to the precious metal, making Co_3O_4 a good replacement catalyst candidate for ORR. The catalytic activity was attributed to Co^{3+} well distributed in the nanostructure.

Plasma based deposition methods can also be used for deposition of cobalt oxide films. Jirátová et al. [15] deposited Co_3O_4 films on steel meshes using magnetron sputtering with Ar + O_2 gas added to the chamber and tested the materials for catalysis of oxidation of ethanol with considerably higher catalytic performance compared to Co_3O_4 nano-pellets. Jozwiak et al. [16] used chemical vapor deposition (CVD) method for deposition of cobalt oxide sandwich structure. These films exhibited significant activity for ORR and OER.

As mentioned previously, cobalt oxides can also be synthesized by electrochemical processes, commonly known as anodization, without annealing at high temperature. This process involves the electrochemical dissolution of the native oxide on top of a metallic material and formation of a thin layer of protective oxides. By changing the anodization potential, different oxides and hydroxides can be obtained. One drawback of this method is that it is only applicable to conductive materials. Aluminum and titanium, both in bulk and as nanostructured materials, are often processed in this manner [17,18]. Using this method, catalysts can be synthesized in different forms, such as nanoparticles, but also to functionalize film surfaces. Anodization processes have been developed for cobalt oxides as thin films on pure Co [19–21] and on various substrates [22]. In this work, we apply this method to a thin film and combine it with catalysis testing. The film is modified to become catalytically active by room temperature oxidation in the same testing solution as for ORR testing.

In the present study, cobalt thin films were sputter-deposited onto steel substrates and modified electrochemically to form cobalt oxide particles on top of the surface. These oxide particles were tested for ORR activity by different electrochemical methods (cyclic voltammetry and chronoamperometry) in alkaline electrolyte. The material system was found to be rapidly reactive when oxygen was introduced into the solution and had high activity for ORR. Thus, these results demonstrate that anodized cobalt thin films can be a suitable candidate as electrocatalyst for water recombination applications.

2. Materials and methods

2.1. Thin film growth

The Co films were deposited using magnetron sputtering using a metallic cobalt target (purity 99.95%, Plasmaterials) onto 1 mm thick plates of low-alloyed steel (C 0.08 wt%; Si 0.02 wt%; Mn 0.52 wt%; Al 0.04 wt%; Cr 0.04 wt%; Fe balance). Depositions were performed in an ultra-high vacuum chamber (base pressure below 4×10^{-7} Pa) at room temperature. The target power was set to 100 W, the argon flow to 2.67×10^{-1} Pa (2 mTorr) and the deposition time was 20 min during which the sample was rotating in the chamber to ensure homogeneous deposition.

Prior to deposition, the substrates were polished with SiC paper and diamond paste to obtain a final surface finish of 0.25 μm (mirror polished). Then the substrates were ultrasonically cleaned with ethanol and finally rinsed with acetone.

2.2. Material characterization

The morphology and chemical composition were analyzed using scanning electron microscopy (SEM) Sigma 300 VP Gemini (Zeiss, 5 kV accelerating voltage), and an energy dispersive spectroscopy (EDS) detector (Oxford Instruments X-MAx^N) integrated in the microscope. For cross-section analysis, samples were mounted in epoxy, then polished with SiC paper and diamond paste to obtain a final surface finish of 0.25 μm. The crystal structure of the coatings was characterized with X-ray diffraction (XRD) in a θ-2θ configuration using Cu Kα radiation (λ = 1.5406 Å). Crystallography Open Database files COD 9012950 for Co and COD 1538531 for Co_3O_4 were used to identify the phases.

X-ray photoelectron spectroscopy (XPS) was used for elemental analysis and assessment of chemical bonding. O1 s and Co 2p core level spectra were recorded using an Axis Ultra DLD instrument from Kratos Analytical (UK) employing monochromatic Al Kα radiation (hν = 1486.6 eV) and an anode power of 150 W. The base pressure during spectra acquisition was lower than 1.5×10^{-7} Pa (1.1×10^{-9} Torr). No charge compensation was used during analyses. The analyzer pass energy was set to 20 eV resulting in the full width at half maximum of 0.55 eV for the Ag $3d_{5/2}$ peak of calibration Ag sample. All spectra were collected at normal emission angles. The area analyzed by XPS is 0.3×0.7 mm^2. As the commonly used charge referencing method relying on the C 1s peak of adventitious carbon is not reliable [23], all spectra are referenced to the metallic Co component of the Co $2p_{3/2}$ spectrum set at 778.3 eV [24]. Spectra deconvolution and quantification is performed using CasaXPS software package (version 2.3.16) and sensitivity factors supplied by the instrument manufacturer. After linear background subtraction the core level spectra were fitted using, Gaussian functions. The model constraints include: (i) the full-width-at-half-maximum (FWHM) is the same for all peaks, (ii) 2:1 intensity ratios are preserved between $2p_{3/2}$ and $2p_{1/2}$ spin-split components in the Co 2p spectrum, (iii) the binding energy splitting between $2p_{3/2}$ and $2p_{1/2}$ components in the Co 2p spectrum is fixed.

2.3. Electrochemical oxidation and measurements

Electrochemical oxidation (anodization) and measurements were carried out in a cell with a three-electrode setup: the Co film was the working electrode, the reference electrode was a saturated calomel electrode (SCE), −0.24 V vs the standard hydrogen electrode (SHE), and the counter electrode was a Pt wire. A PARSTAT 3000A-DX potentiostat was used to control and measure currents and potentials. 1 M KOH (pH ~ 14) was used as electrolyte.

The Co films were anodized through a potential-step experiment. The potential was initially set to −1 V vs SCE for 5 min, and then increased up to +0.15 V for 20 min.

The scan rate for cyclic voltammograms (CV) and linear scan voltammograms (LSV) was 5 mV/s. Samples were cycled at least 10 times to get uniform and stable CV before recording the data. For ORR tests, the electrolyte was saturated with oxygen, and the oxygen flow was maintained in the solution during tests to ensure saturation. For oxygen-free testing, the solution was purged for 30 min with nitrogen gas prior to the measurements. All measurements were repeated on duplicate samples.

The kinetics of the electrochemical reactions were calculated using the Tafel equation:

$$E = A + B\,log(j) \quad (1)$$

where E is the potential, j is the current density, A and B are the parameters to be determined from the log (j) vs E plots; A is the intercept at the origin, and B is the Tafel slope, frequently used to compare catalysts with one another.

3. Results

3.1. Thin film characterization before and after oxidation

Surface and cross-sectional analysis of the as-deposited Co film was carried out by SEM and is shown in Fig. 1(a) and (b). The films are smooth and continuous with only minor defects or porosities across the substrates and have a thickness of ~400 nm. In Fig. 1(a), lines are observed which are remaining scratches after the polishing steps of the substrate. An interface region, darker area in SEM image, can be observed in Fig. 1(b). This region is where the film has been detached during cross-section preparation, due to poor adhesion of the film to the steel substrate.

After deposition, the Co film was anodized to obtain the catalytically active cobalt oxide. Fig. 1(c) and (d) show SEM images of the obtained oxide particles on top of the film. A suitable anodization potential was selected by recording cyclic voltammograms from −0.8 V to 0.2 V vs SCE with a scan rate of 5 mV/s, shown in Fig. 2(a). Two distinctive peaks were found at −0.58 V (A1) and +0.13 V (A2). A1 corresponds to the Co/Co^{2+} couple and involves the formation of $Co(OH)_2$. A2 is associated with the couple $Co(OH)_2/Co_3O_4$ [20]. The absence of cathodic peaks on the reverse scan indicates that the oxidation reaction is irreversible.

In the potential-step measurement, the oxidation potential was set to 0.15 V vs SCE to ensure that the potential region where the oxidation can occur was reached. The current response to the potential step is featured in the Fig. 2(b). The negative cathodic current corresponds to the removal of the passive oxide layer formed after deposition. The positive anodic current corresponds to the oxidation of Co. The anodic current is quite low in comparison to the cathodic current but steady over time, indicating a slow continuous oxidation.

After anodization, a slight color shift from metallic grey to light blue could be observed macroscopically on the Co film, confirming that a reaction had taken place. On the microscopic level, the film was covered with thin, hexagonal particles, see Fig. 1(c–d). According to the EDS data, in the areas between the particles the film has not been oxidized and remain as metallic Co. Nevertheless, small pore-like features have appeared, which could be from the dissolution of Co to form the oxide particles. At higher magnification [Fig. 1(d)] it can be observed that the particles have a plate-like structure with hexagonal morphology and an upwards orientation. The plate-like particles are approximately 400 nm in diameter, and a few nanometers thick. Their composition, according to EDS analysis, are Co (58 at.%) and O (42 at.%). While these results should not be overinterpreted since EDS is rather inaccurate for light elements like oxygen, this ratio suggests the formation of cobalt oxides, CoO_x, with a slight excess of Co compared to the Co_3O_4 structure.

Fig. 3 shows X-ray diffractograms of the as-deposited Co film, the anodized film, and the steel substrate. The steel substrate is composed of polycrystalline iron with a body centred cubic crystal structure. The cobalt coating shows the expected hexagonal closed packed structure of Co metal. The main peaks for Co correspond to the (100) and (101) planes (identified with COD file). The other peaks from the Co reference are missing, indicating the film has a dual preferred orientation. A new peak at 19° in the diffractogram, corresponding to the (111) peak of Co_3O_4, was detected after anodization of the film. The (222) peak for Co_3O_4 overlaps with a substrate peak at 40° and they could not be distinguished.

XPS analysis was performed to confirm the formation of cobalt oxides. The Co 2p and O 1s core level spectra obtained from anodized samples are shown in Fig. 4.

In the Co 2p spectrum, Co $2p_{3/2}$ and Co $2p_{1/2}$ peaks corresponding to three different oxidation states of Co atoms were identified. The lowest BE peaks with $2p_{3/2}$ and $2p_{1/2}$ spin-split components at 778.3 eV and 793.5 eV, respectively, correspond to the Co—Co bond from the metallic

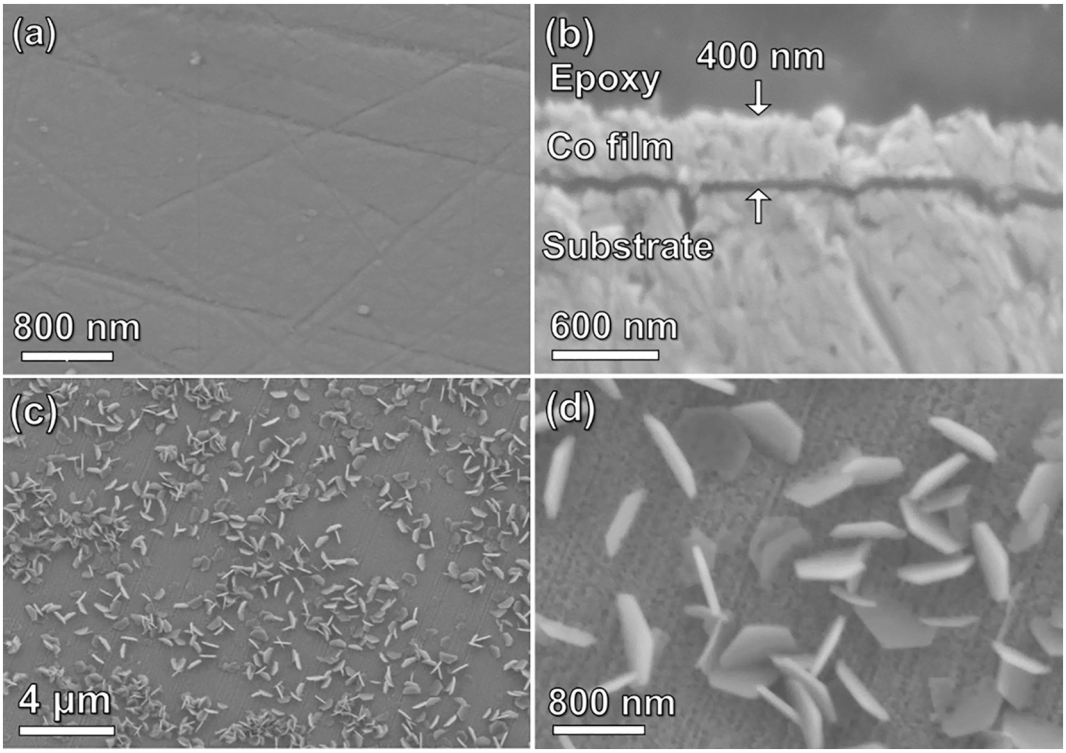

Fig. 1. SEM micrographs of (a) surface and (b) cross-section of Co film deposited on steel substrate, and (c–d) film surface covered with Co oxide particles after anodization.

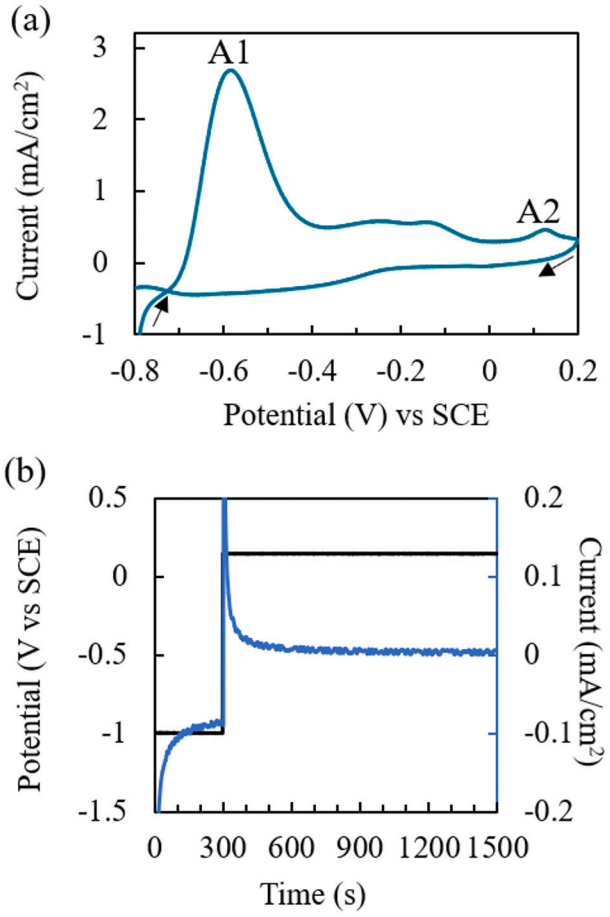

Fig. 2. (a) Cyclic voltammogram for Co thin film in 1 M KOH, scan rate 5 mV/s (arrows indicate scan direction) and (b) potential (black curve) and current profiles (blue curve) over time during anodization. (For interpretation of the references to color in this figure legend, the reader is referred to the web version of this article.)

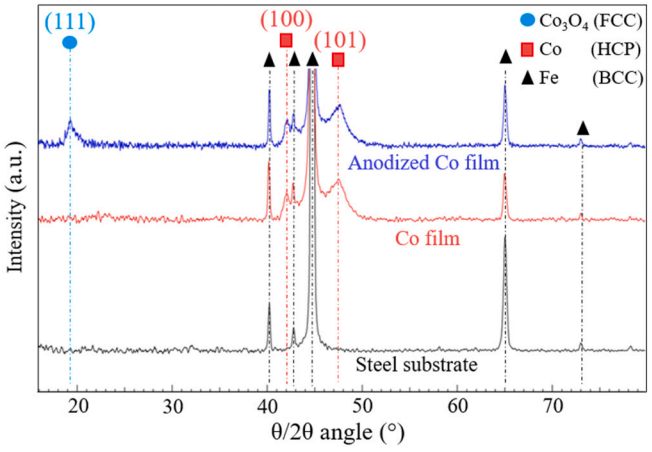

Fig. 3. XRD diffractograms of the steel substrate (black), as-deposited Co film (red), and anodized Co film (blue). (For interpretation of the references to color in this figure legend, the reader is referred to the web version of this article.)

Co film beneath the Co oxide particles. The second pair of $2p_{3/2}$-$2p_{1/2}$ peaks is found at 780.0 and 795.1 eV and is assigned to Co^{2+}. The third pair of $2p_{3/2}$-$2p_{1/2}$ peaks is found at 781.5 and 796.9 eV and is assigned to Co^{3+} [25]. Broad features in the region between 784 and 792 eV, and 799 and 809 eV are satellite peaks possibly due to photoionization

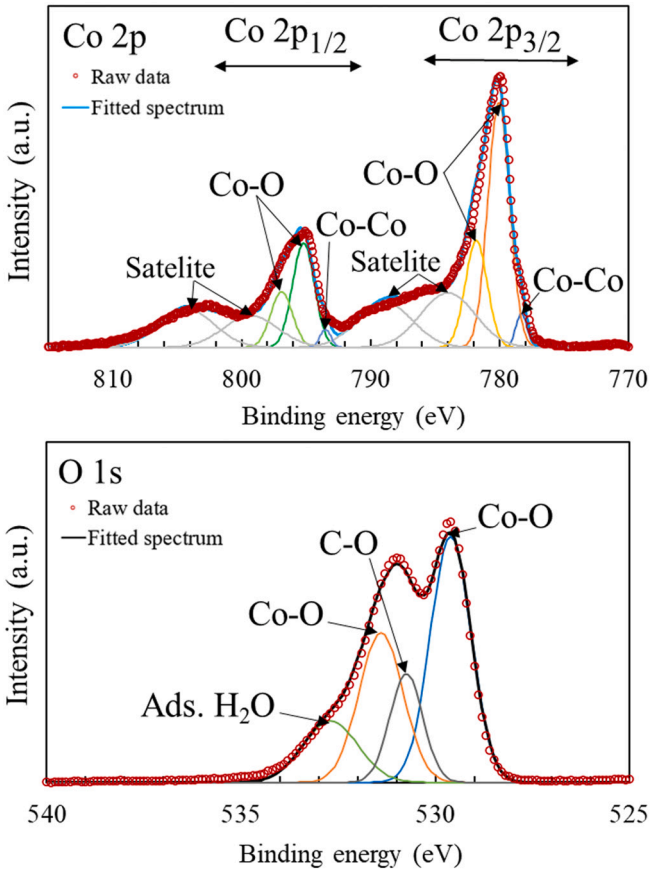

Fig. 4. XPS spectra for anodized sample, Co 2p and O 1s with baseline correction and fitted spectra. Multiple peaks are observed due to different oxidation states of Co in the spinel structure.

events associated with the presence of Co oxides [26,27]. This shows that there is a mix of Co^{2+} and Co^{3+}, the two cations present in the spinel structure of Co_3O_4. In the corresponding O 1s spectrum, the lowest BE peak at 529.6 eV corresponds to a Co—O bond and a second peak at 531.4 eV shows a Co—O bond with a higher oxidation state [27,28]. Apart from the Co oxide peaks the O 1s spectrum contains also contributions from surface contamination, as samples are measured in the as received state. The peak at 530.7 eV corresponds to bonds between carbon and oxygen, e.g. C—O or O=C—O components [28,29], and the shoulder at 532.7 eV is due to the water adsorbed onto the surface [29].

3.2. Electrocatalytic activity

The catalytic activity of the oxide films towards ORR was evaluated using CV. The steel substrate was used as reference. The anodized films were tested in oxygen-free solution (purged with N_2) and in a solution saturated with oxygen. The results are presented in Fig. 5(a).

The contribution from the substrate is negligible since the current density is very low (maximum −0.02 mA/cm^2 at −0.50 V) in the oxygen-rich environment. For the anodized films in oxygen-free solution, the current density for ORR is very low (−0.07 mA/cm^2 at −0.50 V), compared to in oxygen-rich solution where the current density was nearly 10 times higher (−0.6 mA/cm^2 at −0.50 V). The cathodic current increases at −0.25 V which corresponds to the start of ORR activity. As the current increase solely is observed in oxygen-rich environment, it is clear that the current response is due to ORR activity. The continuous increase of current after the ORR potential (−0.3 V vs SCE) is likely due to a coupled-reaction taking place after the catalytic activity as it is not observed in the oxygen-free solution.

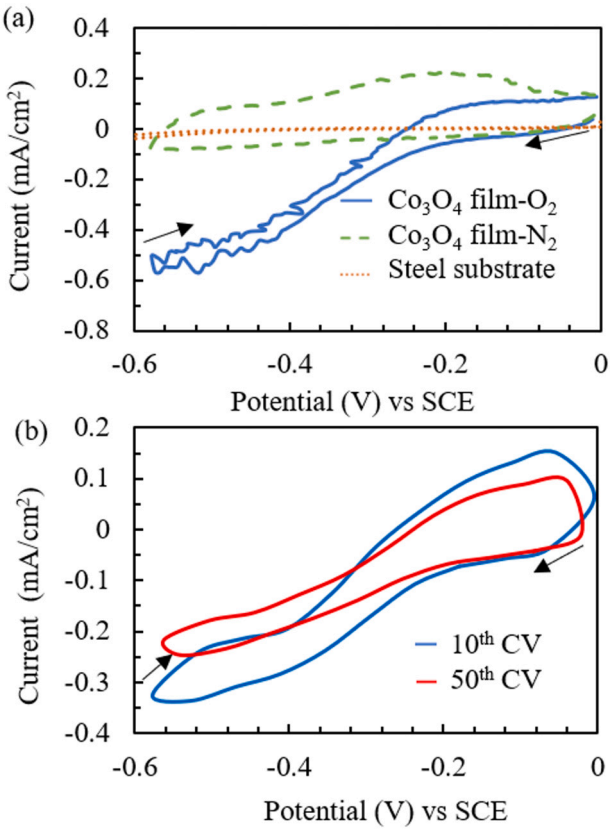

Fig. 5. CVs for anodized Co film (a) in oxygen rich solution (blue curve), oxygen free solution (green curve) and for substrate in oxygen rich solution (orange curve) (b) after 10 ORR cycles (blue curve) and after 50 ORR cycles (red curve), scan rate 5 mV/s. (For interpretation of the references to color in this figure legend, the reader is referred to the web version of this article.)

From the data obtained in the CV curves in Fig. 5(a), the Tafel slope for the ORR reaction was calculated to 226 mV/decade using Eq. (1).

CV was repeated for 50 cycles to follow the catalytic activity over time, see Fig. 5(b). The maximum current decreases slightly over time, from −0.32 to −0.25 mA/cm^2 at −0.50 V, but the evolution of current density with the potential remains the same.

Chronoamperometry at −0.4 V vs SCE was carried out to study the ORR behaviour over time. Oxygen was inserted to the electrolyte after 5 min. The current as a function of time is shown in Fig. 6. It is seen that the current for the anodized film increased rapidly until 15 min where the rate decreased and reached the current maximum value of −0.35 mA/cm^2. After 30 min, the current decreased slowly to −0.25 mA/cm^2.

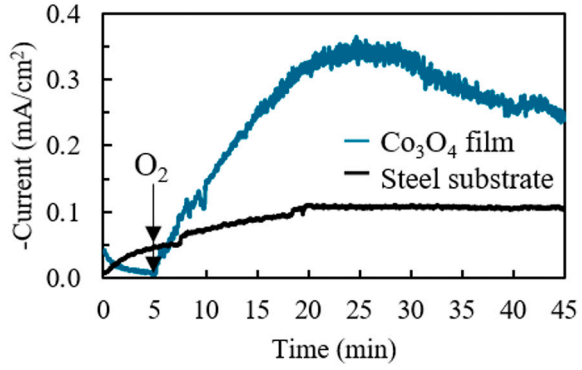

Fig. 6. Current (mA/cm^2) for the steel substrate and the anodized film over time with applied −0.4 V vs SCE. Oxygen gas was introduced into the solution after 5 min.

The anodized Co film has a three times higher current response for ORR activity compared to the substrate, meaning the reduction of oxygen occurs more efficiently with the film and the material system has a higher reactivity with oxygen.

3.3. Film characteristics after electrocatalytic testing

After ORR evaluation, the films were characterized with SEM, EDS and XPS again. Fig. 7(a–b) shows SEM micrographs of the cobalt oxide film after one linear scan voltammetry (LSV) from 0 V to −0.58 V in 1 M KOH saturated with O_2.

The particles on top of the film after the catalytic reaction are similar to those observed after anodization in terms of morphology and composition [Fig. 1(c), (d)]. The Co film beneath, however, has a higher oxygen content (18 at.% O) after one LSV than before LSV. Fig. 7(c, d) shows SEM micrographs of the cobalt oxide film after 50 cycles in 1 M KOH saturated with oxygen. The morphology of the particles on top of the film is also similar to the ones after anodization. However, EDS analysis revealed that the hexagons have a higher oxygen content 60 at.% O, implying that the excess of Co after anodization has now been fully oxidized to Co_3O_4. The film beneath has become covered with small whiskers, enriched in oxygen (O 48 at.% and Co 52 at.%). This composition is close to that of the particles after anodization.

Fig. 7(e, f) show SEM micrographs of the sample after the chronoamperometry measurement, current vs time with applied potential −0.4 V vs SCE. Larger particles (1–2 μm in diameter) have formed in addition to the oxide particles (400 nm in diameter) observed for the other samples. EDS analysis shows that these larger particles have a higher oxygen content compared to the smaller ones (66 at.% O and 55 at.% O, respectively). The smaller particles are Co_3O_4 with no Co excess and the larger ones likely consist of CoO_2. In between the particles, whiskers with a composition close to Co_3O_4 (61 at.% O, 39 at.% Co) have grown. Altogether, there is a clear indication of particle growth and oxidation when a potential is applied in an oxygen-rich environment.

The XPS O 1s normalized spectra for the anodized film, after one LSV and after 50 CVs are presented in Fig. 8. After the first LSV, and even more after 50 cycles, the relative intensity of the O 1s peak at 531.4 eV, corresponding to Co—O bonding with a higher oxidation state, increases with respect to the signal from the anodized film (black curve).This further confirms that the surface becomes more oxidized when a potential is applied with time. This can be correlated with the full oxidation of Co in the particles to form Co_3O_4 and the growth of the oxide layer beneath the particles.

To summarize the results, Table 1 shows the EDS data collected from the oxide particles and the remaining Co film beneath them. The oxygen content of the particles and especially of the film beneath them, increases after the ORR measurements, a clear sign of progressive oxidation of the film surface.

4. Discussion

4.1. Electrochemical oxidation of cobalt thin films

Co films as deposited were smooth and covering the whole substrate, even the features left from substrate polishing. When the films are immersed into the alkaline solution, Co can start to dissolve and form Co^{2+} ions. These ions can then be oxidized either into cobalt hydroxides or cobalt oxides. By applying a potential, the equilibrium of the system is disturbed in a controlled manner and the oxidation reactions become thermodynamically favourable, and therefore the system can be modified into the desired compounds. The first surface modifications in this work were carried out with a potential-step measurement. Initially, the potential was set to −1 V vs SCE to remove the passive film, instantaneously formed in air after deposition, to have a pure layer of Co. Then, the potential was increased to 0.15 V vs SCE (anodic potential) to

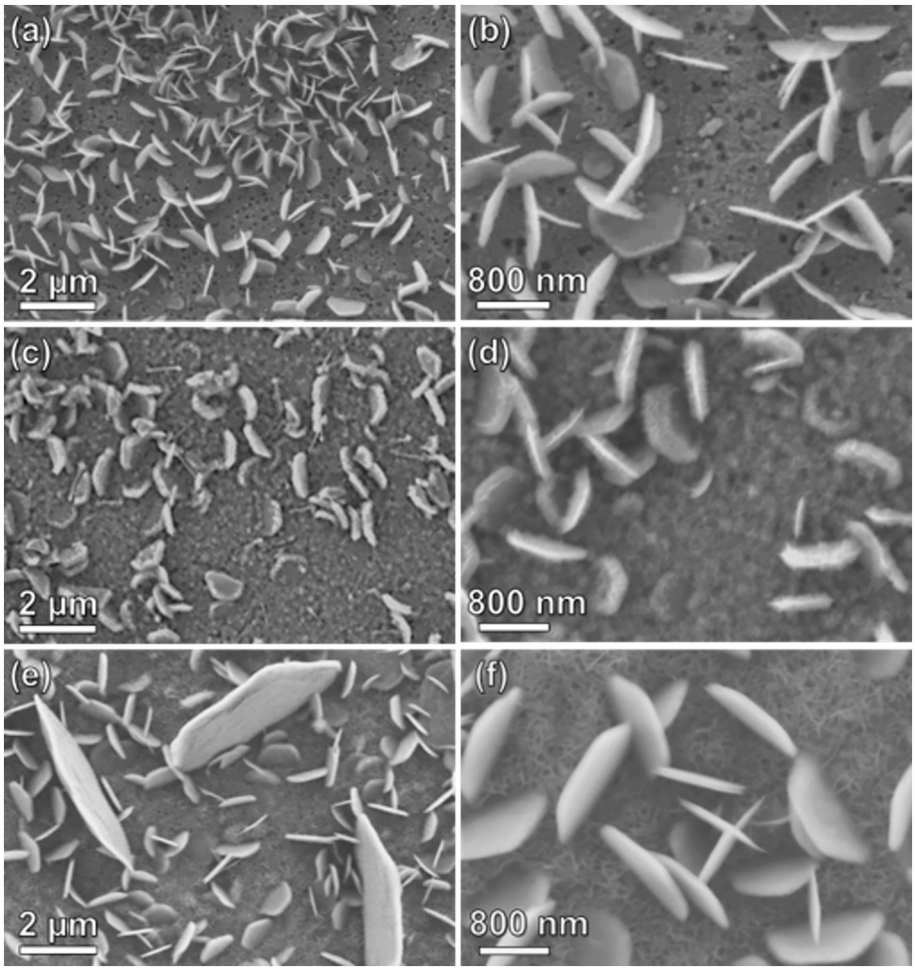

Fig. 7. SEM micrographs of anodized Co film after (a, b) one LSV and (c, d), 50 CVs of ORR (e, f) chronoamperometry measurement with applied potential (e) shows the larger particles, (f) shows the smaller particles.

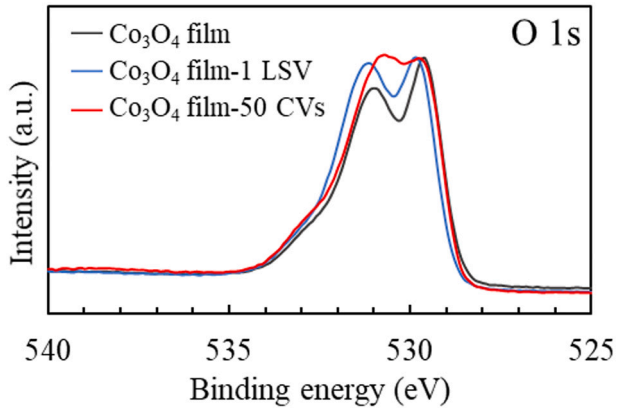

Fig. 8. XPS O 1s normalized spectra for anodized Co film (red curve), after one LSV (blue curve) and after 50 ORR cycles (black curve). (For interpretation of the references to color in this figure legend, the reader is referred to the web version of this article.)

oxidize the surface. In the SEM image [Fig. 1(d)], pore-like features were observed on the film surface, which could be from the dissolution of Co to form the oxide particles. This process has been studied before by Gallant et al. [21] who performed the anodization of pure Co discs in $NaHCO_3$ solution at pH 8. They identified the oxide layer as double layered Co_3O_4 and CoO, with Co_3O_4 as the thinnest and outer layer.

Table 1
EDS data from oxides particles and the remaining film beneath them for the different electrochemical measurements.

		Co (at.%)	O (at.%)	Standard deviation
Anodized particles	Particles	58	42	±0.96
	Film	99	<1	±0.06
1 LSV	Particles	58	42	±0.81
	Film	82	18	±1.02
50 cycles	Particles	40	60	±1.08
	Film	52	48	±0.85
Chronoamperometry	Particles	39	61	±1.01
	Film	43	57	±1.34

Their results are comparable to those of Ohtsuka et al. [30] who showed the formation of two layers on Co rods in a borate solution (pH 8.4). In the Pourbaix diagram for Co and H_2O [14], the stability window of Co_3O_4 in basic pH is found in the range of −0.2 V to 1.2 V vs SHE. This suggests that Co oxide, Co_3O_4, is formed at the second peak observed in the CV [A2 in Fig. 2] as 0.13 V vs SCE corresponds to 0.37 V vs SHE. Our CV results are similar to those reported by other research groups, with two passivity regions, A1 corresponds to Co^{2+}/Co and the formation of $Co(OH)_2$ and A2 to the further oxidation of Co^{2+} into Co^{3+} in Co_3O_4 [20,21].

Several mechanisms for the formation of cobalt oxides have been proposed. From $Co(OH)_2$ precursors, Casella et al. suggested the following reaction [31]:

$$3\ Co(OH)_2 + 2\ OH^- \rightarrow Co_3O_4 + 4\ H_2O + 2\ e^-$$

while Liang et al. proposed that [32]:

$$3\ Co^{2+} + 8\ OH^- \rightarrow Co_3O_4 + 4\ H_2O + 2\ e^-$$

which is a reaction from cobalt salts without the formation of cobalt hydroxides, and correlates better to the state of the depassivated film before the oxidation.

From the EDS data (Table 1), it is clear that the particles formed on top of the Co film are Co oxides with a slight excess of Co, meaning that Co is not fully oxidized into its common oxide forms CoO or Co_3O_4. In the XPS spectrum [Fig. 4], Co $2p^{3/2}$ and Co $2p^{1/2}$ peaks are present and also some contribution from Co—Co bonds can be identified. This indicates that both of Co^{2+} and Co^{3+} are present in the material lattice after anodization. The presence of two oxidation states indicates the formation of a spinel structure [33] and not a cobalt hydroxide or CoO (species with Co^{2+} cations only). The transition into higher oxidation states when a potential is applied has also been demonstrated by in-situ XPS studies. Strehblow et al. [20] studied cobalt discs in 0.1 M NaOH, at 0.3 V vs SHE, where the signal for Co^{3+} was much higher compared to lower potentials; Co^{2+} was also present.

The XRD patterns [Fig. 3] of the anodized film has a small new peak compared to the pure Co film, which corresponds to the (111) peak of Co_3O_4. This also proves that the surface was oxidized during the anodization process to form the spinel structure. The absence of other Co_3O_4 peaks [(220) and (311) at around 30° and 38°, respectively] suggests a preferential orientation of the oxide particles along the [111] direction [5]. Hexagonal particles are a stable shape for Co_3O_4 [34] since they will tend to minimize their formation energy by growing with exposed {111} facets [35]. The hexagonal shape of the particles can be surprising since Co_3O_4 is a cubic system, but this shape has been observed by other authors [5] [25,34–36]. The standing basal planes observed in the SEM images [Fig. 1(d)] are likely an effect of growth kinetics. For layered materials in general [37,38], growth along basal planes occurs much faster than perpendicularly. If standing basal planes nucleate, they can therefore rapidly outgrow parallel-growing planes.

Our study shows that hexagonally shaped cobalt oxide particles are formed on top of the Co film. Gallant et al. [21] showed instead a uniform Co_3O_4 layer on top of the grounded Co discs. This discrepancy can be due to limited surface diffusion because of the structure and surface energy of the film compared to bulk discs. Hydrothermal processes, involving calcination or annealing of precursors at high temperature, for the synthesis of Co_3O_4 result into nano-particles shaped as either spherical, rectangular or hexagonal particles ranging from 10 to 200 nm in diameter [5,35,36]. Electrolytes or solvents such as NaOH or DMF, have shown to be able to reorganise the Co^{2+} ions dissolved in a solution [4]. This could mean that KOH has such a role for the Co^{2+} ions dissolved from the Co film. Since dissolution occurs close to the surface of the film under applied potential, the ions are not likely to diffuse away, causing oxidation to occur closer to the surface and form oxide particles anchored to the film. The oxidation in alkaline solutions with applied potential has also been observed by Mathankumar et al. [34], where the grains of Co_3O_4 particles deposited on glass substrates grew after potentiostatic exposure of the oxide film (1.59 V vs RHE, 0.5 V vs SCE) in 1 M KOH for 12 h. The particles were hexagonal plates and in the μm range. In our study the applied potential was lower and resulted into smaller particles but with a similar morphology to reported materials.

4.2. Catalytic mechanism

The active sites for ORR in the Co oxides are likely to be the Co^{3+} ions, which can adsorb oxygen molecules and then serve as electron transfer media to form OH^- ions. The electron transfer can involve four electrons according to the following reaction:

$$O_2(ads) + 2\ H_2O + 4e^- \leftrightarrow 4OH^-$$

or two times two electrons with the intermediate formation of peroxide ions [5].

In previous studies, the electron number for ORR in KOH has been reported to be close to 4 (by Koutecky-Levich plot analysis), indicating the reaction takes the direct pathway [4,5,13,33]. It can be assumed that the direct pathway is also taken for the anodised film. In the same studies, Co^{3+} has been reported as the active sites in Co_3O_4, as the cations can adsorb oxygen by chemisorption. The presence of Co^{3+} ions in the oxide particles synthesized in this study was confirmed by XPS analysis, thus the ORR is most likely to take place on these cations.

The shape of our CVs has, unlike CVs reported in literature [5,13,26,32], no distinctive peak for the ORR. Most studies report the start of ORR activity at 0.9 V vs RHE and the position of the ORR peak for Co_3O_4 at 0.85 V vs RHE which corresponds to −0.15 V and −0.2 V vs SCE, respectively. By comparing these values with the present study, we can deduce that there is a 0.1 V overpotential for the anodized Co films, thus the ORR peak should take place at −0.3 V vs SCE.

The continuous increase of current could be explained by a follow-up reaction involving oxidation and growth of the layer beneath the particles described in the next section.

4.3. Coupled reactions during electrochemical measurements

The electrochemical measurements were carried out in an oxygen-rich environment and with an applied potential to disturb the equilibrium of the system and promote oxidation. CVs show that after the ORR potential region, the current continues to increase instead of decreasing to form a peak. This behaviour was not observed in oxygen-free solutions, indicating it must be a follow-up or coupled reaction to the ORR. After the first LSV, the area of the film between the oxide particles was slightly oxidized (18 at.% from EDS data) and the peak for oxygen bonds in the XPS analysis [Fig. 8] at higher binding energies was increased in intensity compared to the anodized sample. In all, this shows that oxidation of the film has been initiated. After 50 cycles of ORR, the particles no longer have any excess of Co and indicate the completed transformation into Co_3O_4 particles. The film beneath them was covered with needle-like whiskers, with a composition close to the particles after anodization. We propose a mechanism for this continuous oxidation as following: the remaining metallic cobalt continues to dissolve into Co^{2+} ions and the applied potential inhibits the diffusion of the ions outwards. The presence of oxygen in the solution and the applied potential make oxidation favourable until the film becomes fully covered with Co oxides. Moreover, during ORR Co^{3+} adsorbs oxygen and serves as electron transfer media [5]. This adsorption could also lead to further oxidation of the particles as it has been seen in the XPS profiles with increased intensity for the Co-bond with higher oxidation state after ORR. The reactions proposed in the previous sections could have taken place even though it is not in the same potential range.

When a constant potential of −0.4 V vs SCE was applied, the particles on the surface had grown much larger compared to after 50 CVs. The formation of whiskers with the same composition as particles after anodization again indicates that the surface continued to oxidize. The particles might have merged together in the process to form larger oxide particles. According to Mathankumar et al. [34], the growth of Co_3O_4 particles was observed after having applied a potential over time. This indicates that under applied potential and oxygen-rich conditions the initially formed oxide particles can be further oxidized and even form larger particles during the ORR study.

4.4. Kinetics of catalyst and performances

The ORR kinetics of Co-oxide particles was evaluated through chronoamperometry experiments [Fig. 6] and Tafel slopes extracted from CVs. The electrolyte was however unstirred and the electrode stationary. Therefore, the results cannot be directly compared with rotation disc electrodes (RDE) studies. The catalysts are active towards

ORR and have an immediate current response when oxygen is introduced to the solution in the kinetic study over time [Fig. 6]. Reduction of oxygen efficiently takes place on the particles and reaches a maximum limit after 15 min of exposure to oxygen. After this limit the current is stable for ~10 min, and then decreases from −0.35 mA/cm^2 to −0.25 mA/cm^2. This decrease of current is believed to be due to the coupled reactions described above, involving oxidation and growth of particles.

The Tafel slope of 226 mV/decade is high compared to previous observations in literature. For example, Shinagawa et al. [39] calculated a Tafel slope for Pt in KOH, of 60 mV/decade. Xiao et al. [33] studied Co_3O_4 grown on graphene and a slope of 84–116 mV/decade was obtained. A high Tafel slope indicates slower kinetics for the electron transfer. The specific surface area of particles on a 2D film is considerably lower than that of nanoparticles grown on graphene, meaning there is less active material available for the catalytic reaction which could explain the difference in Tafel slopes. Nevertheless, the oxide particles on the thin film have presented current responses, meaning the electron transfer is successfully carried out.

The anodized Co film was submitted to 50 CVs cycles to study the performances of the catalyst over time. The CV has the same shape as after 10 cycles and is in the same current range. However, there is a slight decrease of current from −0.32 mA/cm^2 to −0.25 mA/cm^2 [Fig. 5 (b)] meaning that the activity of the catalyst has attenuated over time, probably caused by the coupled oxidation of the films during ORR.

5. Conclusions

The present work demonstrates that sputtered Co thin films can be modified by anodization to become catalysts for ORR and water recombination applications in KOH solutions. Cobalt oxides, Co_3O_4, were synthesized electrochemically on the surface of Co films. The oxide was observed to grow as hexagonal platelets. The oxide platelets were evaluated as electrocatalysts for reduction of oxygen in alkaline solution. In cyclic voltammograms a −0.7 mA/cm^2 cathodic current was obtained and in experiments with applied potential a stable maximum of −0.35 mA/cm^2 was measured for over 10 min. In both cases the response of the oxide platelets to oxygen and its reduction was rapid and stable. However, post-characterization of the different samples revealed that the surface had been modified during the experiments and was fully covered with cobalt oxides with a higher oxidation state then initially after the anodization process. Nevertheless, this process has proven to be a way of functionalising surfaces, the oxide film clearly increased the catalytic activity of the steel substrate; and one step closer to the replacement of noble metals in technologies driven by water recombination.

CRediT authorship contribution statement

Clara Linder: Conceptualization, Investigation, Data curation, Formal analysis, Writing - original draft. **Smita Gangaprasad Rao:** Investigation, Writing - review & editing. **Arnaud le Febvrier:** Investigation, Writing - review & editing. **Grzegorz Greczynski:** Investigation, Formal analysis, Writing - review & editing. **Rune Sjövall:** Conceptualization, Writing - review & editing. **Sara Munktell:** Conceptualization, Supervision, Writing - review & editing. **Per Eklund:** Conceptualization, Supervision, Writing - review & editing, Funding acquisition. **Emma M. Björk:** Project administration, Conceptualization, Supervision, Writing - review & editing, Funding acquisition.

Declaration of competing interest

The authors declare that they have no known competing financial interests or personal relationships that could have appeared to influence the work reported in this paper.

Acknowledgments

This work was supported by the competence center FunMat-II funded by the Swedish Agency for Innovation Systems (VINNOVA, grant no 2016-05156), and the VINNOVA grant no 2018-04291. We also acknowledge the Swedish Government Strategic Research Area in Materials Science on Functional Materials at Linköping University (Faculty Grant SFO-Mat-LiU No. 2009 00971).

References

[1] Y. Wang, D.F. Ruiz Diaz, K.S. Chen, Z. Wang, X.C. Adroher, Materials, technological status, and fundamentals of PEM fuel cells – a review, Mater. Today 32 (2020) 178–203, https://doi.org/10.1016/j.mattod.2019.06.005.
[2] X. Ge, A. Sumboja, D. Wuu, T. An, B. Li, F.W.T. Goh, T.S.A. Hor, Y. Zong, Z. Liu, Oxygen reduction in alkaline media: from mechanisms to recent advances of catalysts, ACS Catal. 5 (2015) 4643–4667, https://doi.org/10.1021/acscatal.5b00524.
[3] S. Sønderby, T. Klemensø, B.H. Christensen, K.P. Almtoft, J. Lu, L.P. Nielsen, P. Eklund, Magnetron sputtered gadolinia-doped ceria diffusion barriers for metal-supported solid oxide fuel cells, J. Power Sources 267 (2014) 452–458, https://doi.org/10.1016/j.jpowsour.2014.05.101.
[4] J. Xu, P. Gao, T.S. Zhao, Non-precious Co3O4 nano-rod electrocatalyst for oxygen reduction reaction in anion-exchange membrane fuel cells, Energy Environ. Sci. 5 (2012) 5333–5339, https://doi.org/10.1039/c1ee01431e.
[5] P.W. Menezes, A. Indra, D. Gonza, N.R. Sahraie, I. Zaharieva, M. Schwarze, P. Strasser, H. Dau, M. Driess, High-performance oxygen redox catalysis with multifunctional cobalt oxide nanochains: morphology-dependent activity, ACS Catal. 5 (2015) 2017–2027, https://doi.org/10.1021/cs501724v.
[6] C. Chen, Y. Kang, Y. Li, N. Markovic, G.A. Somorjai, P. Yang, R. Stamenkovic, Highly crystalline multimetallic nanoframes with three-dimensional electrocatalytic, Science (80-.) 343 (2014) 1339–1343, https://doi.org/10.1126/science.1249061.
[7] Y. Li, Q. Li, H. Wang, L. Zhang, D.P. Wilkinson, J. Zhang, Recent progresses in oxygen reduction reaction electrocatalysts for electrochemical energy applications, Electrochem. Energy Rev. 2 (2019) 518–538, https://doi.org/10.1007/s41918-019-00052-4.
[8] X. Huang, Y. Wang, W. Li, Y. Hou, Noble metal-free catalysts for oxygen reduction reaction, Sci. China Chem. 60 (2017) 1494–1495, https://doi.org/10.1007/s11426-017-9153-6.
[9] L. Han, S. Dong, E. Wang, Transition-metal (Co, Ni, and Fe)-based electrocatalysts for the water oxidation reaction, Adv. Mater. 28 (2016) 9266–9291, https://doi.org/10.1002/adma.201602270.
[10] P.C.M. Hamdani, R.N. Singh, Co3O4 and Co-based spinel oxides bifunctional oxygen electrodes, Int. J. Electrochem. Sci. 5 (2010) 556–577.
[11] G. Zhang, C. Li, J. Liu, L. Zhou, One-step conversion from metal–organic frameworks to Co3O4@N-doped carbon nanocomposites towards highly efficient frameworks to Co3O4@N-doped carbon nanocomposites towards highly efficient oxygen reduction catalysts, J. Mater. Chem. A 2 (2014) 8184–8189, https://doi.org/10.1039/c4ta00677a.
[12] X. Xia, M. Li, T. Liu, P. Liang, X. Huang, Facile synthesis of cobalt oxide as electrocatalyst for the oxygen reduction reaction in microbial fuel cells, Chem. Eng. J. 342 (2018) 395–400, https://doi.org/10.1016/j.cej.2018.02.092.
[13] Y. Liang, Y. Li, H. Wang, J. Zhou, J. Wang, Co3O4 nanocrystals on graphene as a synergistic catalyst for oxygen reduction reaction, Nat. Mater. 10 (2011) 780–786.
[14] M. Cassir, L. Mendoza, J. Chivot, T. Pauporté, C. Mansour, New insight in the behaviour of Co–H2O system at 25–150°C, based on revised Pourbaix diagrams, Corros. Sci. 50 (2007) 62–69, https://doi.org/10.1016/j.corsci.2007.07.002.
[15] K. Jirátová, R. Perekrestov, M. Dvořáková, J. Balabánová, P. Topka, M. Koštejn, J. Olejníček, M. Čada, Z. Hubička, F. Kovanda, Cobalt oxide catalysts in the form of thin films prepared by magnetron sputtering on stainless-steel meshes: performance in ethanol oxidation, Catalysts 9 (2019), https://doi.org/10.3390/catal9100806.
[16] L. Jozwiak, J. Balcerzak, A. Kubiczek, J. Tyczkowski, Plasma deposited thin-film sandwich-like bifunctional electrocatalyst for oxygen reduction and evolution reactions, Thin Solid Films 660 (2018) 161–165, https://doi.org/10.1016/j.tsf.2018.06.002.
[17] F. Zhang, J. Evertsson, F. Bertram, L. Rullik, F. Carla, M. Långberg, E. Lundgren, J. Pan, Integration of electrochemical and synchrotron-based X-ray techniques for in-situ investigation of aluminum anodization, Electrochim. Acta 241 (2017) 299–308, https://doi.org/10.1016/j.electacta.2017.04.154.
[18] J. Venturini, F. Bonatto, W.C. Guaglianoni, T. Lemes, S. Arcaro, A.K. Alves, C. P. Bergmann, Cobalt-doped titanium oxide nanotubes grown via one-step anodization for water splitting applications, Appl. Surf. Sci. 464 (2019) 351–359, https://doi.org/10.1016/j.apsusc.2018.09.093.
[19] C.Y. Lee, K. Lee, P. Schmuki, Anodic formation of self-organized cobalt oxide nanoporous layers, Angew. Chem. Int. Ed. 52 (2013) 2077–2081, https://doi.org/10.1002/anie.201208793.
[20] J. Sinclair, R.P. Frankenthal, E. Kálamán, W. Plieth, Corrosion and Corrosion Protection, 2001, https://doi.org/10.1016/0003-6870(73)90259-7.
[21] D. Gallant, M. Pézolet, S. Simard, Optical and physical properties of cobalt oxide films electrogenerated in bicarbonate aqueous media, J. Phys. Chem. B 110 (2006) 6871–6880, https://doi.org/10.1021/jp056689h.

[22] S.D. Sartale, V. Ganesan, C.D. Lokhande, Electrochemical deposition and characterization of CoFe2O4 thin films, Phys. Status Solidi Appl. Mater. Sci. 202 (2005) 85–94, https://doi.org/10.1002/pssa.200406898.
[23] G. Greczynski, L. Hultman, Compromising science by ignorant instrument calibration—need to revisit half a century of published XPS data, Angew. Chem. Int. Ed. 59 (2020) 5002–5006, https://doi.org/10.1002/anie.201916000.
[24] J.F. B.K. Moulder, W.F. Stickle, P.E. Sobol, X-ray Photoelectron Spectroscopy (XPS), 1992, https://doi.org/10.1002/0470014229.ch22.
[25] S.Y. Zhang, T.T. Li, H.L. Zhu, Y.Q. Zheng, Co3O4 polyhedrons with enhanced electric conductivity as efficient water oxidation electrocatalysts in alkaline medium, J. Mater. Sci. 53 (2018) 4323–4333, https://doi.org/10.1007/s10853-017-1855-2.
[26] L. Liu, Z. Jiang, L. Fang, H. Xu, H. Zhang, X. Gu, Y. Wang, Probing the crystal plane effect of Co3O4 for enhanced electrocatalytic performance toward efficient overall water splitting, ACS Appl. Mater. Interfaces 9 (2017) 27736–27744, https://doi.org/10.1021/acsami.7b07793.
[27] M.C. Biesinger, B.P. Payne, A.P. Grosvenor, L.W.M. Lau, A.R. Gerson, R.S.C. Smart, Resolving surface chemical states in XPS analysis of first row transition metals, oxides and hydroxides: Cr, Mn, Fe, Co and Ni, Appl. Surf. Sci. 257 (2011) 2717–2730, https://doi.org/10.1016/j.apsusc.2010.10.051.
[28] L.S. Sundar, G.O. Irurueta, E. Venkata Ramana, M.K. Singh, A.C.M. Sousa, Thermal conductivity and viscosity of hybrid nanfluids prepared with magnetic nanodiamond-cobalt oxide (ND-Co3O4) nanocomposite, Case Stud. Therm. Eng. 7 (2016) 66–77, https://doi.org/10.1016/j.csite.2016.03.001.
[29] G. Greczynski, L. Hultman, Self-consistent modelling of X-ray photoelectron spectra from air-exposed polycrystalline TiN thin films, Appl. Surf. Sci. 387 (2016) 294–300, https://doi.org/10.1016/j.apsusc.2016.06.012.
[30] T. Ohtsuka, N. Sato, Two-layer formation of passivating films on cobalt in neutral solution, J. Electrochem. Soc. 128 (1981) 2522–2528, https://doi.org/10.1149/1.2127284.
[31] I.G. Casella, M. Gatta, Study of the electrochemical deposition and properties of cobalt oxide species in citrate alkaline solutions, J. Electroanal. Chem. 534 (2002) 31–38, https://doi.org/10.1016/S0022-0728(02)01100-2.
[32] Y. Liang, H. Wang, P. Diao, W. Chang, G. Hong, Y. Li, Oxygen reduction electrocatalyst based on strongly coupled cobalt oxide nanocrystals and carbon nanotubes, J. Am. Chem. Soc. 134 (2012) 15849–15857, https://doi.org/10.1021/ja305623m.
[33] J. Xiao, Q. Kuang, S. Yang, F. Xiao, S. Wang, L. Guo, Surface structure dependent electrocatalytic activity of Co3O4 anchored on graphene sheets toward oxygen reduction reaction, Sci. Rep. 3 (2013) 1–8, https://doi.org/10.1038/srep02300.
[34] M. Mathankumar, S. Anantharaj, A.K. Nandakumar, S. Kundu, B. Subramanian, Potentiostatic phase formation of β-CoOOH on pulsed laser deposited biphasic cobalt oxide thin film for enhanced oxygen evolution, J. Mater. Chem. A 5 (2017) 23053–23066, https://doi.org/10.1039/c7ta07410g.
[35] X.Y. Yu, Q.Q. Meng, T. Luo, Y. Jia, B. Sun, Q.X. Li, J.H. Liu, X.J. Huang, Facet-dependent electrochemical properties of Co3O4 nanocrystals toward heavy metal ions, Sci. Rep. 3 (2013) 1–7, https://doi.org/10.1038/srep02886.
[36] X. Zhou, F. Chen, F. Cao, W. Shen, J. Liu, X. Xu, Nanostructured hexagonal cobalt oxide plates and their electrochemical properties, Mater. Lett. 180 (2016) 175–178, https://doi.org/10.1016/j.matlet.2016.05.136.
[37] J. Frodelius, J. Lu, J. Jensen, D. Paul, L. Hultman, P. Eklund, Phase stability and initial low-temperature oxidation mechanism of Ti 2AlC thin films, J. Eur. Ceram. Soc. 33 (2013) 375–382, https://doi.org/10.1016/j.jeurceramsoc.2012.09.003.
[38] L.P.H. Jeurgens, W.G. Sloof, F.D. Tichelaar, E.J. Mittemeijer, Growth kinetics and mechanisms of aluminum-oxide films formed by thermal oxidation of aluminum, J. Appl. Phys. 92 (2002) 1649–1656, https://doi.org/10.1063/1.1491591.
[39] T. Shinagawa, A.T. Garcia-esparza, K. Takanabe, Insight on Tafel slopes from a microkinetic analysis of aqueous electrocatalysis for energy conversion, Nat. Publ. Gr. 5 (2015) 1–21, https://doi.org/10.1038/srep13801.